

# $WZ$ plus missing- $E_T$ signal from gaugino pair production at LHC7

Howard Baer<sup>1\*</sup>, Vernon Barger<sup>2†</sup>, Sabine Kraml<sup>3‡</sup>, Andre Lessa<sup>4‡</sup>,  
Warintorn Sreethawong<sup>1§</sup> and Xerxes Tata<sup>5¶</sup>

<sup>1</sup>*Dept. of Physics and Astronomy, University of Oklahoma, Norman, OK 73019, USA*

<sup>2</sup>*Dept. of Physics, University of Wisconsin, Madison, WI 53706, USA*

<sup>3</sup>*Laboratoire de Physique Subatomique et de Cosmologie, UJF Grenoble 1, CNRS/IN2P3, INPG, 53 Avenue des Martyrs, F-38026 Grenoble, France*

<sup>4</sup>*Instituto de Física, Universidade de São Paulo, São Paulo-SP, Brazil*

<sup>5</sup>*Dept. of Physics and Astronomy, University of Hawaii, Honolulu, HI 96822, USA*

## Abstract

LHC searches for supersymmetry currently focus on strongly produced sparticles, which are copiously produced if gluinos and squarks have masses of a few hundred GeV. However, in supersymmetric models with heavy scalars, as favored by the decoupling solution to the SUSY flavor and  $CP$  problems, and  $m_{\tilde{g}} \gtrsim 500$  GeV as indicated by recent LHC results, chargino-neutralino ( $\tilde{W}_1^\pm \tilde{Z}_2$ ) production is the dominant cross section for  $m_{\tilde{W}_1} \sim m_{\tilde{Z}_2} < m_{\tilde{g}}/3$  at LHC with  $\sqrt{s} = 7$  TeV (LHC7). Furthermore, if  $m_{\tilde{Z}_1} + m_Z \lesssim m_{\tilde{Z}_2} \lesssim m_{\tilde{Z}_1} + m_h$ , then  $\tilde{Z}_2$  dominantly decays via  $\tilde{Z}_2 \rightarrow \tilde{Z}_1 Z$ , while  $\tilde{W}_1$  decays via  $\tilde{W}_1 \rightarrow \tilde{Z}_1 W$ . We investigate the LHC7 reach in the  $WZ + \cancel{E}_T$  channel (for both leptonic and hadronic decays of the  $W$  boson) in models with and without the assumption of gaugino mass universality. In the case of the mSUGRA/CMSSM model with heavy squark masses, the LHC7 discovery reach in the  $WZ + \cancel{E}_T$  channel becomes competitive with the reach in the canonical  $\cancel{E}_T + \text{jets}$  channel for integrated luminosities  $\sim 30 \text{ fb}^{-1}$ . We also present the LHC7 reach for a simplified model with arbitrary  $m_{\tilde{Z}_1}$  and  $m_{\tilde{W}_1} \sim m_{\tilde{Z}_2}$ . Here, we find a reach of up to  $m_{\tilde{W}_1} \sim 200$  (250) GeV for 10 (30)  $\text{fb}^{-1}$ .

PACS numbers: 14.80.Ly, 12.60.Jv, 11.30.Pb

---

\*Email: baer@nhn.ou.edu

†Email: barger@pheno.wisc.edu

‡Email: sabine.kraml@lpsc.in2p3.fr

‡Email: lessa@fma.if.usp.br

§Email: wstan@nhn.ou.edu

¶Email: tata@phys.hawaii.edu

# 1 Introduction

A major goal of the CERN Large Hadron Collider (LHC) is to test the idea of weak scale supersymmetry (SUSY) [1], wherein superpartners of the Standard Model (SM) particles have masses of the order of 1 TeV. The SUSY searches by the ATLAS and CMS collaborations have reported no signal beyond SM expectations [2, 3] in  $\sim 1 \text{ fb}^{-1}$  of data. Interpreting their results within the mSUGRA/CMSSM model [4], ATLAS and CMS exclude roughly the mass range  $m_{\tilde{q}} \sim m_{\tilde{g}} \lesssim 1 \text{ TeV}$  for  $m_{\tilde{q}} \simeq m_{\tilde{g}}$ , and  $m_{\tilde{q}} \lesssim 550 \text{ GeV}$  in the case where  $m_{\tilde{q}} \gg m_{\tilde{g}}$ .<sup>1</sup> This reach will soon be extended since each experiment now has  $\sim 5 \text{ fb}^{-1}$  of data collected. Analysis of this extended data sample is eagerly anticipated by the HEP community.

Within a large class of SUSY models, it is expected that pair production of strongly interacting sparticles— $\tilde{g}\tilde{g}$ ,  $\tilde{g}\tilde{q}$  and  $\tilde{q}\tilde{q}$  production—constitutes the dominant SUSY production cross sections [6, 7]. The gluinos and squarks are then expected to decay through a (possibly lengthy) cascade to lighter sparticles plus SM particles, until the decay chain terminates in the (stable) lightest SUSY particle (LSP) [8]. The LSP is expected from cosmological arguments to be a massive, neutral, weakly interacting particle (such as the lightest neutralino  $\tilde{Z}_1$ ) and so does not deposit energy in the experimental apparatus, giving rise to the classic missing transverse energy ( $\cancel{E}_T$ ) signature. Thus, gluino and squark pair production followed by cascade decays is expected to give rise to final states containing multiple isolated leptons, multiple jets and  $\cancel{E}_T$  [9].

While weak scale supersymmetric models are theoretically very compelling, they do suffer from a variety of problems, including 1. the SUSY flavor problem, 2. the SUSY  $CP$  problem, 3. the gravitino problem, and 4. the danger of too rapid proton decay in SUSY grand unified theories (GUTs). All four of these problems are greatly ameliorated if not solved by the decoupling solution, wherein first and second generation sfermion masses are pushed into the multi-TeV regime or even beyond. Naturalness may be maintained in models wherein sparticles that couple directly to the Higgs sector—the third generation scalars and electroweak-inos—remain at or below the TeV scale [10, 11]. Also, in many SUSY models, it is expected that gaugino mass parameters unify at the GUT scale, in parallel with unification of gauge couplings. Renormalization group running effects result in weak scale gaugino masses occurring in the approximate ratio  $M_1 : M_2 : M_3 \sim 1 : 2 : 7$ . We would thus expect the physical gluino  $\tilde{g}$ , the wino-like chargino  $\tilde{W}_1$  and the bino-like neutralino  $\tilde{Z}_1$  to be found with roughly the same mass ratio, provided the superpotential  $\mu$ -parameter  $|\mu| \gg M_2$ . Consequently, in models with gaugino mass unification, the experimental bounds on the gluino mass impose severe constraints on chargino and neutralino masses. Current analyses do not put independent constraints on the electroweak-ino masses if the gaugino mass unification condition is dropped [12]. Moreover, the relative strengths of signals in various multilepton topologies (as well as the gluino mass reach if the parent-daughter mass difference is sufficiently small) depend sensitively on the  $\tilde{g} - \tilde{Z}_1$  and/or  $\tilde{g} - \tilde{W}_1$  mass differences. Finally, an independent discovery of directly produced charginos and neutralinos is essential to elucidate the supersymmetry origin of any excess in the well-studied multilepton plus multijet plus  $\cancel{E}_T$  channel at the LHC. It is therefore interesting

---

<sup>1</sup>To be precise, in the mSUGRA/CMSSM interpretation, squark masses are varied up to  $m_{\tilde{q}} \lesssim 2 \text{ TeV}$ , giving a gluino mass limit of about  $m_{\tilde{g}} \gtrsim 700 \text{ GeV}$ ; this limit suffers further weakening for decoupling scalars: see [5].

and relevant to find ways to discover charginos and neutralinos independently of gluinos.

Another point is important to note: as we push the gluino mass to larger values, convolution of the  $\tilde{g}\tilde{g}$  subprocess cross sections with parton distribution functions (PDFs) requires sampling higher and higher values of parton fractional momentum  $x_F$ . For such high values of  $x_F$ , the parton-parton luminosity is sharply falling. At some point we expect that, despite being strongly-produced, gluino pair production will no longer dominate over electroweak-ino pair production, since these latter reactions will sample the PDFs at much lower values of  $x_F$  if electroweak-inos are significantly lighter than gluinos.

To illustrate this, we plot in Fig. 1 the  $\tilde{g}\tilde{g}$ ,  $\tilde{W}_1^\pm\tilde{Z}_2$  and  $\tilde{W}_1^+\tilde{W}_1^-$  production cross sections in pb at LHC with  $pp$  collisions at  $\sqrt{s} = 7$  TeV. Our results are in NLO QCD from the program Prospino [13]. We take  $m_{\tilde{q}} \simeq 15$  TeV for the first and second generations, in accord with a decoupling solution to the above-mentioned pathologies and, for simplicity, assume universal gaugino masses at the GUT scale. From Fig. 1, we see that gluino-pair production is dominant for  $m_{\tilde{g}} \lesssim 500$  GeV. For higher values of  $m_{\tilde{g}}$ ,  $\tilde{W}_1^\pm\tilde{Z}_2$  production is dominant, followed by  $\tilde{W}_1^+\tilde{W}_1^-$  production (the reaction  $\tilde{W}_1^\pm\tilde{Z}_1$  has lower cross section,<sup>2</sup> as can be seen *e.g.* in Fig. 12.23 of Ref. [1]). For LHC with  $\sqrt{s} = 14$  TeV,  $\tilde{g}\tilde{g}$  production remains dominant up to  $m_{\tilde{g}} \sim 1$  TeV if squarks are very heavy. Since ATLAS and CMS already exclude  $m_{\tilde{g}} \lesssim 550$  GeV when  $m_{\tilde{q}}$  is large it may prove fruitful to probe electroweak gaugino pair production in the 2011 data but most of all in the 2012 LHC run. This was recognized early on in [6, 7] and also more recently in [14, 15]. Recognizing that the stability of the Higgs sector also requires sub-TeV top squarks, we also show the cross section for top squark pair production for  $m_{\tilde{t}_1} = m_{\tilde{g}}$  by the dotted line<sup>3</sup> in Fig. 1. We see that this cross section also drops off rapidly with the top squark mass. Unless top squarks are exceptionally light (with masses of order  $m_{\tilde{W}_1}$  or smaller, and certainly much smaller than  $m_{\tilde{g}}$ ), electroweak-ino production remains the dominant mechanism.

Let us next examine the signatures resulting from  $\tilde{W}_1\tilde{Z}_2$  production. If  $m_{\tilde{Z}_2} < M_Z + m_{\tilde{Z}_1}$ , the well-known trilepton signal provides a golden signature for chargino-neutralino production [7, 16] provided only that the branching fraction for neutralino decay is not unduly suppressed [17]. The two-body chargino decay  $\tilde{W}_1 \rightarrow \tilde{Z}_1 W$  is expected to dominate for  $m_{\tilde{W}_1} \gtrsim M_W + m_{\tilde{Z}_1}$ , while the two-body decay  $\tilde{Z}_2 \rightarrow \tilde{Z}_1 Z$  dominates for  $M_Z + m_{\tilde{Z}_1} \lesssim m_{\tilde{Z}_2} \lesssim m_h + m_{\tilde{Z}_1}$ . For even higher values of  $m_{\tilde{Z}_2}$ , i.e.  $m_{\tilde{Z}_2} \gtrsim m_{\tilde{Z}_1} + m_h$ , the decay mode  $\tilde{Z}_2 \rightarrow \tilde{Z}_1 h$  turns on and dominates.

This is illustrated in Fig. 2, where we show the  $\tilde{Z}_2$  branching fractions versus  $m_{\tilde{Z}_2}$  for a mSUGRA model line with  $m_0 = 10$  TeV,  $A_0 = -2m_0$ ,  $\tan\beta = 25$  and  $\mu > 0$ . We vary  $m_{1/2}$  to obtain the variation in  $m_{\tilde{Z}_2}$ . In this case,  $\tilde{W}_1\tilde{Z}_2 \rightarrow WZ + \tilde{Z}_1\tilde{Z}_1$  is kinematically allowed for  $175 \text{ GeV} \lesssim m_{\tilde{Z}_2} \lesssim 250 \text{ GeV}$ , which corresponds to gluino masses in the interval  $600 \text{ GeV} \lesssim m_{\tilde{g}} \lesssim 800 \text{ GeV}$ . Thus, in this mass range, we expect the single reaction  $pp \rightarrow \tilde{W}_1\tilde{Z}_2$

<sup>2</sup>For the wino-like  $\tilde{W}_1$  and  $\tilde{Z}_2$ ,  $\tilde{W}_1\tilde{Z}_2$  production occurs via the unsuppressed isotriplet  $W\tilde{W}_1\tilde{Z}_2$  gauge coupling, whereas the  $W\tilde{W}_1\tilde{Z}_1$  coupling is strongly suppressed because it arises only due to the subdominant higgsino content of the wino-like chargino and the bino-like neutralino — the  $W$ -bino-wino coupling is forbidden by gauge invariance.

<sup>3</sup>The LO top squark pair production cross section is determined by QCD and is independent of  $m_{\tilde{g}}$ . In other words, for the dotted line, the graph is plotted versus  $m_{\tilde{t}_1}$ . If other third generation squarks are also light, their pair production cross sections are also given by the dotted line with the understanding that the label on the horizontal axis is the corresponding squark mass.

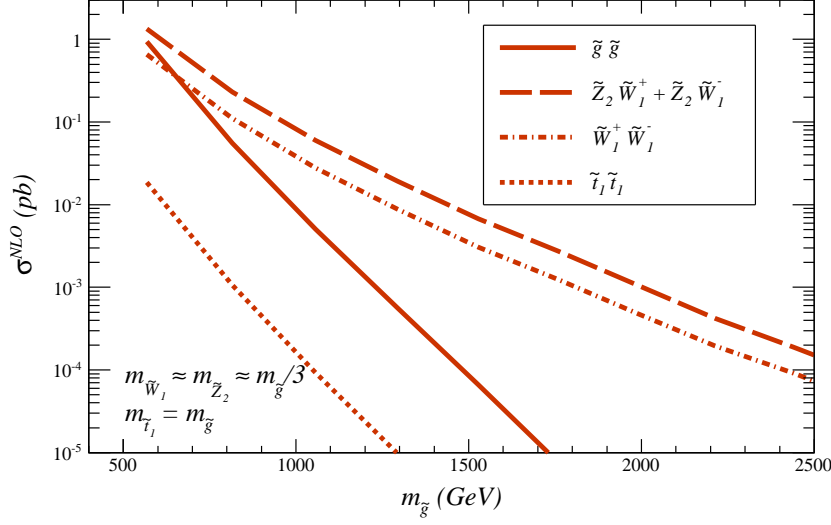


Figure 1: Total NLO cross sections (from Prospino) for  $\tilde{g}\tilde{g}$ ,  $\tilde{W}_1^\pm \tilde{Z}_2$  and  $\tilde{W}_1^+ \tilde{W}_1^-$  production at LHC7 versus  $m_{\tilde{g}}$ , where  $m_{\tilde{q}} = 15$  TeV and  $m_{\tilde{W}_1} \approx m_{\tilde{Z}_2} \approx m_{\tilde{g}}/3$ . The dotted line shows the cross section for  $\tilde{t}_1 \tilde{t}_1$  production with  $m_{\tilde{t}_1} = m_{\tilde{g}}$  and neglecting intra-generational squark mixing.

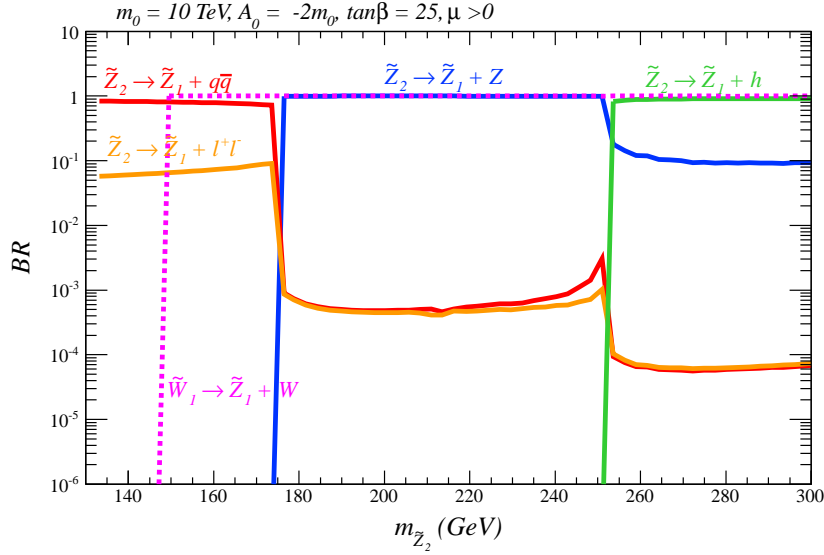


Figure 2: Some prominent branching fractions for  $\tilde{Z}_2$  decay in the  $mSUGRA$  model with parameters  $m_0 = 10$  TeV,  $A_0 = -2m_0$ ,  $\tan\beta = 25$  and  $\mu > 0$ . We also show the  $\tilde{W}_1 \rightarrow W + \tilde{Z}_1$  branching fraction (dotted line).

followed by  $\tilde{W}_1 \rightarrow \tilde{Z}_1 W$  and  $\tilde{Z}_2 \rightarrow \tilde{Z}_1 Z$  to be the dominant SUSY production and decay process at LHC7 for models with full gaugino mass unification. The endpoints of this interval can shift up or down in non-universal mass scenarios.

## 2 Trilepton+ $\cancel{E}_T$ channel

We begin by examining the viability of the reaction  $pp \rightarrow \widetilde{W}_1 \widetilde{Z}_2 \rightarrow WZ + \cancel{E}_T$  for SUSY discovery at LHC7, focusing on the case where both  $Z$  and  $W$  decay leptonically, resulting in clean trilepton events. It is worth mentioning that the trilepton signal from the decay  $\widetilde{Z}_2 \rightarrow \widetilde{Z}_1 Z$  where a pair of opposite-sign same-flavor (OS/SF) dileptons reconstruct the  $Z$  mass has generally been regarded as unobservable because of large SM background from  $WZ$  production. The case where the  $W$  decays hadronically will be discussed in Section 3.

For our LHC7 event generation, we use the event generator Isajet 7.79 [18] for signal reactions, while for the simulation of the background events, we use AlpGen [19] and MadGraph [20] to compute the hard scattering events and Pythia [21] for the subsequent showering and hadronization. In our simulation, we include the following backgrounds for the  $WZ + \cancel{E}_T$  signal:  $t\bar{t}$ ,  $W(\ell\nu)W(\ell\nu)$ ,  $W(\ell\nu)Z(\ell\ell)$ ,  $ZZ$ ,  $W(\ell\nu) + tb$ ,  $Z(\ell\ell) + jets$ ,  $W(\ell\nu) + jets$ ,  $Z(\ell\ell) + b\bar{b}$ ,  $Z(\ell\ell) + t\bar{t}$  and  $W + t\bar{t}$ . For  $t\bar{t}$ ,  $Z + jets$ ,  $W + jets$ ,  $Z + b\bar{b}$  and  $Z + t\bar{t}$  we include the full matrix elements for at least two real parton emissions and use the MLM matching algorithm to avoid double counting. For  $WZ$  production we include the full matrix elements for the  $2 \rightarrow 4$  process  $pp \rightarrow WZ \rightarrow \ell^+ \ell^- \ell' \nu'$ . K-factors for both signal and background<sup>4</sup> (BG) are included and are computed using Prospino [13] and MCFM [22], respectively.

In our calculations, we employ a toy detector simulation with calorimeter cell size  $\Delta\eta \times \Delta\phi = 0.05 \times 0.05$  and  $-5 < \eta < 5$ . The HCAL (hadronic calorimetry) energy resolution is taken to be  $80\%/\sqrt{E} \oplus 3\%$  for  $|\eta| < 2.6$  and FCAL (forward calorimetry) is  $100\%/\sqrt{E} \oplus 5\%$  for  $|\eta| > 2.6$ , where the two terms are combined in quadrature. The ECAL (electromagnetic calorimetry) energy resolution is assumed to be  $3\%/\sqrt{E} \oplus 0.5\%$ . In all these,  $E$  is the energy in GeV units. We use the cone-type Isajet [18] jet-finding algorithm to group the hadronic final states into jets. Jets and isolated lepton are defined as follows:

- Jets are hadronic clusters with  $|\eta| < 3.0$ ,  $R \equiv \sqrt{\Delta\eta^2 + \Delta\phi^2} \leq 0.4$  and  $E_T(jet) > 40$  GeV.
- Electrons and muons are considered isolated if they have  $|\eta| < 2.5$ ,  $p_T(l) > 10$  GeV with visible activity within a cone of  $\Delta R < 0.2$  about the lepton direction,  $\Sigma E_T^{cells} < \min[5, 0.15p_T(l)]$  GeV.
- We identify hadronic clusters as  $b$ -jets if they contain a  $B$  hadron with  $E_T(B) > 15$  GeV,  $|\eta(B)| < 3.0$  and  $\Delta R(B, jet) < 0.5$ . We assume a tagging efficiency of 60% and light quark and gluon jets can be mis-tagged as a  $b$ -jet with a probability 1/150 for  $E_T \leq 100$  GeV, 1/50 for  $E_T \geq 250$  GeV, with a linear interpolation for  $100 \text{ GeV} \leq E_T \leq 250$  GeV.

Next, we invoke the following pre-selection cuts on our signal and background event samples to extract those with a  $\ell^+ \ell^- \ell' + \cancel{E}_T$  topology:

### Pre-Selection Cuts:

- $n(b - jets) = 0$  (to aid in vetoing  $t\bar{t}$  background),
- 3 isolated leptons with  $p_T(\ell) > 20$  GeV and

---

<sup>4</sup>For the background processes where the NLO cross section is not known we take the K-factor to be 1.

- $|m(\ell^+\ell^-) - M_Z| < 10 \text{ GeV}$ ,

where two of the leptons in the event must form an OS/SF pair. If more than one OS/SF pairing is possible, the pair which minimizes  $|m(\ell^+\ell^-) - M_Z|$  is chosen. The remaining lepton is labeled  $\ell'$ .

In Fig. 3 we show the  $\cancel{E}_T$  and transverse mass ( $m_T(\ell', \cancel{E}_T)$ ) distributions for the signal and the SM BG after the pre-selection cuts have been applied. The signal point has  $m_{\tilde{W}_1} = 189.3 \text{ GeV}$ ,  $m_{\tilde{Z}_2} = 187.3 \text{ GeV}$  and  $m_{\tilde{Z}_1} = 89.4 \text{ GeV}$  and we only consider  $\tilde{W}_1\tilde{Z}_2$  production. Due to its relatively light parent mass scale, the signal presents a soft  $\cancel{E}_T$  spectrum, barely visible above the SM background. This is in strong contrast with events from production of the much heavier gluinos or squarks, where the cascade decays to the LSP result in a usually much harder  $\cancel{E}_T$  spectrum. Therefore, the usual  $\cancel{E}_T$  plus jets/leptons searches (optimized to look for strongly produced gluinos and squarks) are insensitive to the  $\tilde{W}_1\tilde{Z}_2$  signal.

As seen in the upper frame of Fig. 3, after the pre-selection cuts the BG is dominated by  $ZZ$  production at low  $\cancel{E}_T$  and by  $WZ$  production for  $\cancel{E}_T \gtrsim 20 \text{ GeV}$ . The transverse mass  $m_T(\ell', \cancel{E}_T)$  from  $W \rightarrow \ell'\nu_{\ell'}$ , shown in the lower frame of Fig. 3, falls sharply beyond the expected Jacobian peak at  $m_T = M_W$ . In contrast, the corresponding signal distribution from  $\tilde{W}_1\tilde{Z}_2$  production extends to considerably larger values due to the presence of the two neutralinos in the final state. Therefore, a  $m_T$  cut is extremely efficient to suppress the  $WZ$  background. This is seen in the lower frame of Fig. 3, where the signal distribution clearly stands out for  $m_T > 100 \text{ GeV}$ . However, since a precise prediction for the  $m_T$  tail from  $WZ$  events requires a full detector simulation or data-driven estimates, we define a conservative signal region requiring:

- $\cancel{E}_T > 50 \text{ GeV}$ ,
- $m_T(\ell', \cancel{E}_T) > 125 \text{ GeV}$ .

The BG cross sections from the dominant SM processes after each of the cuts mentioned above, together with the corresponding cross sections for the representative signal point with  $m_{\tilde{W}_1} = 189.3 \text{ GeV}$ ,  $m_{\tilde{Z}_2} = 187.3 \text{ GeV}$  and  $m_{\tilde{Z}_1} = 89.4 \text{ GeV}$ , are shown in Table 1. We stress that the signal shown in Fig. 3 and listed in Table 1 comes exclusively from  $\tilde{W}_1\tilde{Z}_2$  production. Depending on the sparticle spectrum, the actual signal may be larger if heavier electroweakinos are also accessible, or if gluino and/or squark pair production followed by their cascade decays to the  $WZ$  final state is sizeable. Nonetheless, a trilepton signal would be visible with an integrated luminosity of  $\sim 10 \text{ fb}^{-1}$  at LHC7 even if light electroweakinos are the *only* SUSY particles being produced.

## 2.1 LHC7 Reach

As shown in Table 1 and Fig. 3, for  $m_{\tilde{W}_1} = 189.3 \text{ GeV}$ ,  $m_{\tilde{Z}_2} = 187.3 \text{ GeV}$  and  $m_{\tilde{Z}_1} = 89.4 \text{ GeV}$ , only an excess of  $\sim 2$  events in the trilepton channel (after cuts) would be expected for luminosity of  $\sim 5 \text{ fb}^{-1}$ . Thus larger integrated luminosities are required in order to claim a signal. In Fig. 4, we show the signal significance for various integrated luminosities versus  $m_{\tilde{W}_1}$  (solid lines). For now we use a mSUGRA model line with  $m_0 = 10 \text{ TeV}$ ,  $A_0 = -2m_0$ ,  $\tan\beta = 25$  and  $\mu > 0$ , and we consider the signal only from  $\tilde{W}_1\tilde{Z}_2$  production. To allow for the low signal

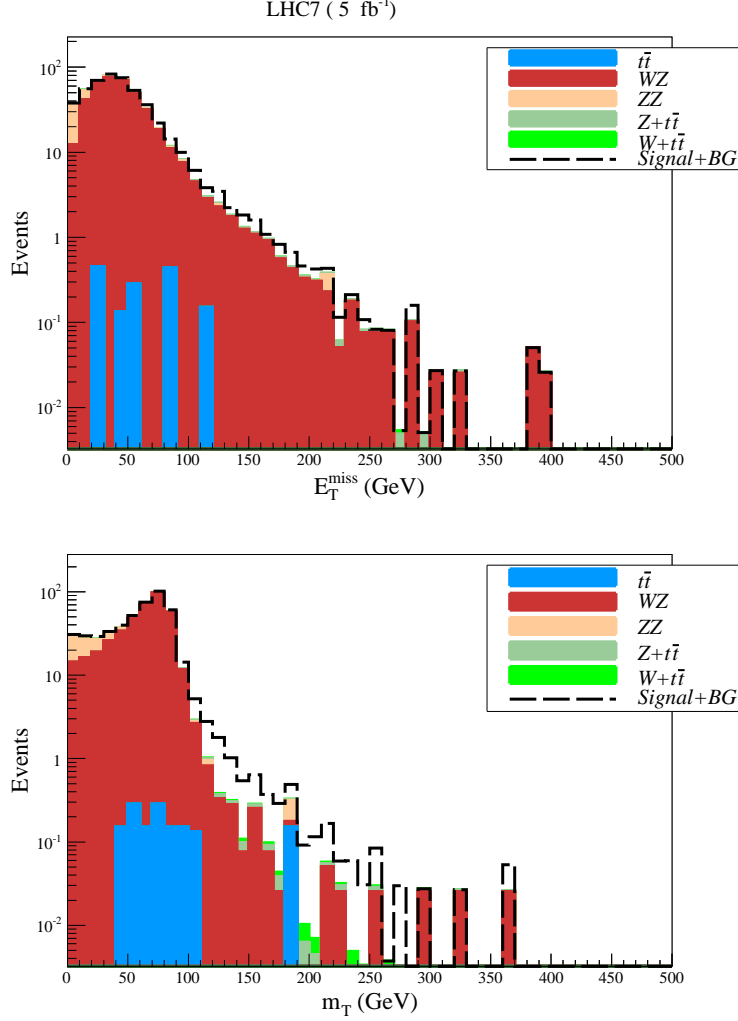


Figure 3:  $\cancel{E}_T$  and transverse mass ( $m_T(\ell')$ ,  $\cancel{E}_T$ ) distributions in  $3\ell + \cancel{E}_T$  events after pre-selection cuts, for an integrated luminosity of  $5 \text{ fb}^{-1}$ . The summed SM backgrounds are shaded while the signal plus background is shown by the dashed histogram. Only the dominant background processes are shown. The signal point has  $m_{\tilde{W}_1} = 189.3 \text{ GeV}$ ,  $m_{\tilde{Z}_2} = 187.3 \text{ GeV}$  and  $m_{\tilde{Z}_1} = 89.4 \text{ GeV}$ .

rates, the significance is computed using Poisson statistics. For  $m_{\tilde{W}_1} \lesssim 170 \text{ GeV}$ , the decay into real  $Z$ s is kinematically forbidden– as shown in Fig. 2– and the signal significance (solid lines) sharply drops in this region. In this case, however, the well-studied trilepton signal mentioned earlier from  $\tilde{W}_1 \tilde{Z}_2 \rightarrow 3\ell + \cancel{E}_T$  where  $m(\ell^+ \ell^-) < M_Z$  is observable. To illustrate this, we show by dashed lines the signal significance, where the same cuts listed in Table 1 are applied, except for the  $m_T$  and  $m(\ell^+ \ell^-)$  cuts. Since in this region  $\tilde{Z}_2$  and  $\tilde{W}_1$  can decay to off-shell  $Z$ s and  $W$ s we require instead:

- $m_T > 0, \quad m(\ell^+ \ell^-) < M_Z - 10 \text{ GeV}$ .



	$t\bar{t}$	$WZ$	$ZZ$	$Z + t\bar{t}$	$W + t\bar{t}$	Total BG	Signal
Events Generated	5.1M	100K	194K	451K	9.5M		200K
Total $\sigma$ (fb)	$1.6 \times 10^5$	$5.1 \times 10^2$	$5.4 \times 10^3$	22.3	183	$7.8 \times 10^6$	$1.1 \times 10^4$
$n(b) = 0, n(l) = 3$	1.6	85.1	9.2	0.9	0.4	97.5	6.7
OS/SF pair	1.1	84.9	9.2	0.9	0.3	96.6	6.7
$m(\ell^+\ell^-)$ cut	0.3	79.1	9.1	0.66	0.06	89.5	6.6
$m_T > 125$ GeV	0.03	0.20	0.03	0.03	0.02	0.31	0.67
$\cancel{E}_T > 50$ GeV	0.03	0.17	0	0.03	0.02	0.25	0.64

Table 1: Number of events generated, total cross section and cross section after cuts for the dominant backgrounds in the trilepton channel and for the signal. All cross sections are in fb and the signal is from just  $\tilde{W}_1\tilde{Z}_2$  production with  $m_{\tilde{W}_1} = 189.3$  GeV,  $m_{\tilde{Z}_2} = 187.3$  GeV and  $m_{\tilde{Z}_1} = 89.4$  GeV. The Total BG values include all processes listed in the text, including the subdominant ones not shown in the Table.

As seen from Fig. 4, we confirm that the signal in the low  $m_{\tilde{W}_1}$  region ( $\lesssim 170$  GeV) is readily observable via this “golden” trilepton channel, due to the large  $\tilde{W}_1\tilde{Z}_2$  production cross sections and small background.<sup>5</sup>

As  $m_{\tilde{W}_1} \simeq m_{\tilde{Z}_2}$  increases so that the  $\tilde{Z}_2 \rightarrow \tilde{Z}_1 Z$  decay turns on, the significance for our  $WZ \rightarrow 3\ell + \cancel{E}_T$  signal increases, reaching its maximum for  $m_{\tilde{W}_1} \sim 220$  GeV. This is due to the fact that, for  $m_{\tilde{W}_1} \lesssim 200$  GeV,  $m_{\tilde{Z}_2} - m_{\tilde{Z}_1} - M_Z \lesssim 15$  GeV and the  $\tilde{Z}_1$ ’s coming from  $\tilde{Z}_2$  decays (and to some extent also those from  $\tilde{W}_1$  decay) are rather soft and so contribute relatively little to both  $\cancel{E}_T$  and to  $m_T$ . As a result, the  $\cancel{E}_T > 50$  GeV and  $m_T > 125$  GeV requirements significantly reduce the signal in this region. As  $m_{\tilde{W}_1}$  increases beyond 220 GeV, the  $\tilde{W}_1\tilde{Z}_2$  production cross section (after cuts) decreases, and so does the signal significance. Finally, once  $m_{\tilde{Z}_2} > m_{\tilde{Z}_1} + m_h$  (at  $m_{\tilde{W}_1} \sim 255$  GeV), the  $\tilde{Z}_2 \rightarrow \tilde{Z}_1 h$  decay turns on and dominates<sup>6</sup> causing the signal to drop sharply.

We remark that for  $5 \text{ fb}^{-1}$  of data, we would expect a  $2\sigma$  effect over essentially the entire region where the decay  $\tilde{Z}_2 \rightarrow \tilde{Z}_1 Z$  dominates. Therefore, the LHC experiments already have accumulated enough luminosity to probe this entire region at  $\sim 95\%$  C.L.! However, in the happy circumstance that some excess is seen in the data,  $\sim 20 - 30 \text{ fb}^{-1}$  of data will be required in order to establish a  $5\sigma$  discovery. This may indeed be achieved in the 2012 run of LHC7. We note further that the SUSY signal events will contain a distinctive asymmetry of trilepton charges  $+(+-)$  *vs.*  $- (+-)$  (where the  $(+-)$  pair reconstructs  $m_Z$ ) that originates from the PDFs since LHC is a  $pp$  collider. In contrast, SM backgrounds from  $t\bar{t}$  and  $Zt\bar{t}$  (but not  $WZ$ ) should have the number of  $+(+-)$  events equal to  $- (+-)$  events, up to statistical fluctuations. In addition, should a large enough data sample be accrued, the  $p_T(Z)$  distribution should be

<sup>5</sup>The valley at the intersection of the solid and dashed lines in Fig. 4 arises because we have different analysis cuts for the two-body and three-body decays of  $\tilde{Z}_2$ . This valley would be smoothed out (and partially filled in) in a treatment that treats  $Z$  as a resonance rather than a particle with a definite mass.

<sup>6</sup>This decay occurs via the Higgs-higgsino-gaugino coupling and so is suppressed by the higgsino content of just one of the two neutralinos. In contrast, the decay to  $Z$  occurs via the doubly suppressed higgsino content of *both* neutralinos.



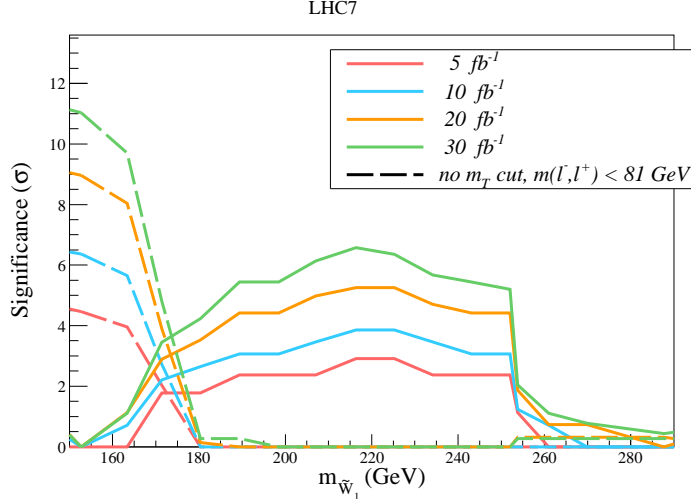


Figure 4: *Significance of  $\tilde{W}_1 \tilde{Z}_2 \rightarrow WZ + \cancel{E}_T \rightarrow 3\ell + \cancel{E}_T$  signal for various integrated luminosities at LHC7. The solid lines have all the trilepton cuts listed in Table 1, while the dashed lines do not include the  $m_T$  cut and require  $M_Z - m(\ell^+ \ell^-) > 10$  GeV instead.*

well-suited for a  $\tilde{Z}_2$  mass extraction since the production and decay modes are single channel.

In Fig. 5, we generalize our results to models with unrelated  $\tilde{W}_1$  and  $\tilde{Z}_1$  masses, *i.e.* models without gaugino mass universality, taking  $m_{\tilde{Z}_2} = m_{\tilde{W}_1}$  and  $\mu \gg M_2$ . In this figure, we show the discovery regions for several integrated luminosities. We require the following discovery criteria:

- significance  $> 5\sigma$ ,
- signal/BG  $> 0.2$  and
- at least 5 signal events.

The mSUGRA model line with  $m_0 = 10$  TeV,  $A_0 = -2m_0$ ,  $\tan\beta = 25$  and  $\mu > 0$ , assumed in Fig. 4, is shown as the dashed orange line. The purple band shows the kinematically allowed region, where  $M_Z < m_{\tilde{Z}_2} - m_{\tilde{Z}_1} < m_h$ . As can be seen, chargino masses up to  $\sim 170$  GeV can already be probed with  $5 \text{ fb}^{-1}$ , if  $m_{\tilde{Z}_1} \lesssim 50$  GeV. As discussed above, for heavier  $\tilde{Z}_1$ , the  $m_{\tilde{Z}_2} - m_{\tilde{Z}_1}$  mass gap reduces, resulting in softer  $m_T$  and  $\cancel{E}_T$  distributions. Therefore the signal efficiency is reduced, requiring higher luminosities in order to achieve  $5\sigma$  significance. This effect is seen throughout the  $m_{\tilde{W}_1}$  vs.  $m_{\tilde{Z}_1}$  plane, rendering the narrow region close to  $m_{\tilde{Z}_2} - m_{\tilde{Z}_1} \sim M_Z$ , where the  $\tilde{Z}_1$  is produced at low  $p_T$ , inaccessible even for  $\mathcal{L} = 30 \text{ fb}^{-1}$ . On the other hand, the region where  $m_{\tilde{Z}_2} - m_{\tilde{Z}_1} \lesssim m_h$  results in boosted  $\tilde{Z}_1$ s and can be easily probed until the decay  $\tilde{Z}_2 \rightarrow \tilde{Z}_1 + h$  turns on, c.f. Fig. 4. The  $30 \text{ fb}^{-1}$  reach extends up to  $m_{\tilde{W}_1} \sim 250$  GeV, for  $m_{\tilde{Z}_1} \lesssim 130$  GeV, covering almost all of the kinematically allowed region for the mSUGRA line with  $m_0 = 10$  TeV,  $A_0 = -2m_0$ . We also show in Fig. 5 a second mSUGRA line with  $m_0 = 1.5$  TeV,  $A_0 = 0$ ,  $\tan\beta = 45$  and  $\mu > 0$ . For these choice of parameters the  $m_{\tilde{Z}_2} - m_{\tilde{Z}_1}$  mass difference is reduced, due to a small (positive)  $A_0$  value

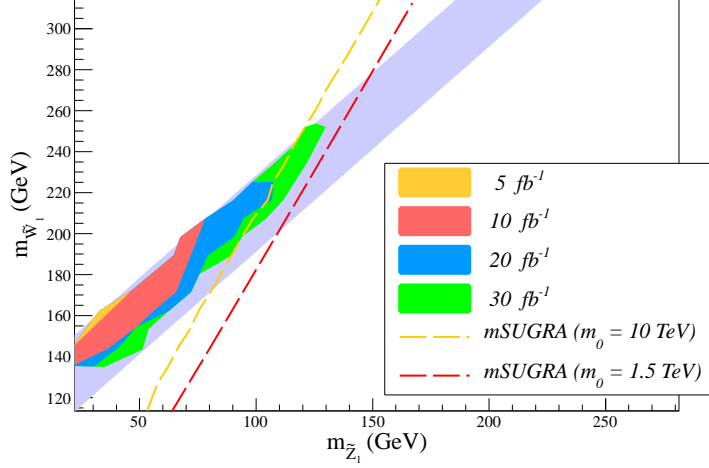


Figure 5:  $5\sigma$  discovery regions for various integrated luminosities at LHC7 in the  $m_{\tilde{W}_1} - m_{\tilde{Z}_1}$  plane. We assume  $m_{\tilde{Z}_2} = m_{\tilde{W}_1}$  and consider only  $\tilde{W}_1\tilde{Z}_2$  production. The Higgs boson mass is assumed to be 128.5 GeV throughout the plane. The orange (red) line shows the mSUGRA line with  $m_0 = 10$  TeV,  $A_0 = -2m_0$ ,  $\tan\beta = 25$  and  $\mu > 0$  ( $m_0 = 1.5$  TeV,  $A_0 = 0$ ,  $\tan\beta = 45$  and  $\mu > 0$ ).

and smaller squark masses. As a result, all of the region where the  $WZ + \cancel{E}_T$  channel is open falls into the inaccessible region at high  $m_{\tilde{Z}_1}$ . However, values of  $A_0 \sim 0$  now seem excluded in mSUGRA if indeed  $m_h$  turns out to be  $\sim 125$  GeV [23].

Up to now we have only considered  $\tilde{W}_1\tilde{Z}_2$  production. Despite having subdominant production cross sections, production of heavier chargino  $\tilde{W}_2$  and neutralinos  $\tilde{Z}_{3,4}$  usually leads to a harder  $\cancel{E}_T$  spectrum due to their cascade decay, possibly enhancing the signal. Furthermore, for low  $m_0$  ( $m_{1/2}$ ) squark (gluino) production and cascade decay can also enhance the trilepton signal. In order to clearly see these effects we choose the  $A_0$  and  $\tan\beta$  values from the red curve in Fig. 5 ( $A_0 = 0$  and  $\tan\beta = 45$ ), where we do not expect the  $\tilde{W}_1\tilde{Z}_2$  signal to be visible for any value of  $m_{1/2}$ , even for  $30 \text{ fb}^{-1}$ . However, now we perform a scan over the  $m_0 - m_{1/2}$  plane and include the production from *all* SUSY particles, including squarks and gluinos. For each point in parameter space, we apply the trilepton cuts shown in Table 1 and take the point to be visible if the discovery criteria listed above are satisfied.

The results are shown in Fig. 6, again for four values of integrated luminosities. All points shown are deemed visible for the corresponding integrated luminosity. The gray regions show the parts of the  $m_0 - m_{1/2}$  plane excluded by theoretical considerations or by experimental constraints. The purple band across the middle of the plot shows the region in parameter space where  $M_Z < m_{\tilde{Z}_2} - m_{\tilde{Z}_1} < m_h$ , while the pink area at low values of  $m_0$  and  $m_{1/2}$  corresponds to the region where at least 50% of the signal comes from gluino and/or squark production. From Fig. 6 we see that, for heavy squarks ( $m_0 > 800$  GeV), the signal mostly comes from electroweakly produced inos. For an integrated luminosity of  $5 \text{ fb}^{-1}$  no points are visible. However, for an integrated luminosity of  $10 \text{ fb}^{-1}$ , the enhancement of the signal from gluino and squark production renders a few points at low  $m_0$  and low  $m_{1/2}$  accessible. For  $20 \text{ fb}^{-1}$  the

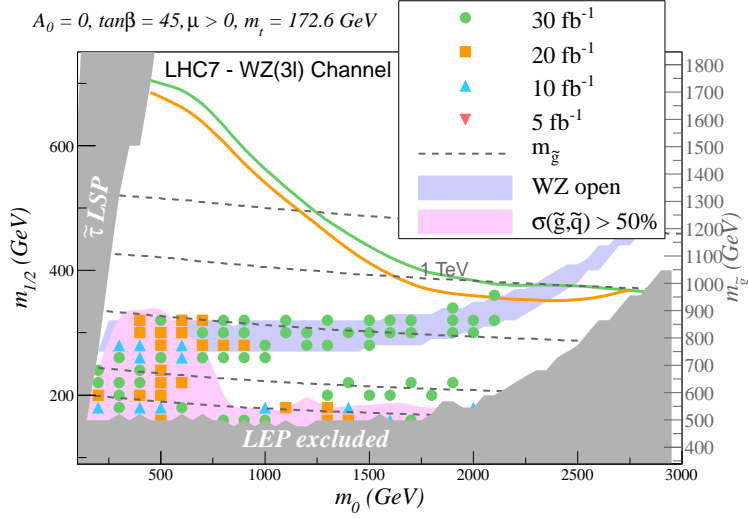


Figure 6: *LHC reach in the  $mSUGRA$  plane for various integrated luminosities for the  $WZ + \cancel{E}_T$  trilepton signal. The pink region is where gluino and/or squark production contribute to at least half the signal, whereas in the purple band the  $WZ + \cancel{E}_T$  channel is accessible via electroweak  $\tilde{W}_1 \tilde{Z}_2$  production. Below the green (orange) solid contours there will be a  $5\sigma$  signal for SUSY via the optimized jets plus  $\cancel{E}_T$  LHC7 search discussed in Ref. [24] for  $30 \text{ fb}^{-1}$  ( $20 \text{ fb}^{-1}$ ).*

reach extends up to  $m_0 \sim 800 \text{ GeV}$  and  $m_{1/2} \sim 300 \text{ GeV}$ . Finally, for  $30 \text{ fb}^{-1}$ , all of the region where the  $WZ + \cancel{E}_T$  channel is open can be probed up to  $m_{1/2} \sim 350 \text{ GeV}$ . In the heavy squark region ( $m_0 > 800 \text{ GeV}$ ), the signal is enhanced by  $\tilde{W}_2$  and  $\tilde{Z}_3$  production, allowing the LHC to probe gluino masses up to  $900 \text{ GeV}$ . We point out that without the enhancement of heavy electroweak-ino production no reach is expected even for  $30 \text{ fb}^{-1}$ , as shown by the red curve in Fig. 5. We note that there are also visible points at low  $m_{1/2}$ , below the  $M_Z < m_{\tilde{Z}_2} - m_{\tilde{Z}_1} < m_h$  band, where the  $\tilde{Z}_2 \rightarrow \tilde{Z}_1 Z$  and  $\tilde{W}_1 \rightarrow \tilde{Z}_1 W$  decays are closed, but  $Z$ s and  $W$ s are still produced from heavier EW-ino decays. It is also worth noting that the focus point (light higgsino) region does not enhance the signal. This is partly due to the more compressed chargino/neutralino spectrum in this region leading to softer  $p_T$  and  $\cancel{E}_T$  [25, 26]. We stress that in Fig. 6 we have only considered observability via  $WZ + \cancel{E}_T \rightarrow \ell^+ \ell^- \ell' + \cancel{E}_T$  and for the region below the “ $WZ$  band” the golden trilepton signal where the OS/SF dilepton pair has a mass below  $M_Z$  can be used as a discovery channel, as shown by the dashed lines in Fig. 4.

We also show in Fig. 6 the optimized LHC7 reach in the jets plus  $\cancel{E}_T$  channel from Ref. [24] (solid lines) for  $\mathcal{L} = 20 \text{ fb}^{-1}$  and  $30 \text{ fb}^{-1}$ . These curves correspond to an optimization over several  $\cancel{E}_T$  plus jets channels with zero leptons and do not include the dedicated cuts for the  $WZ + \cancel{E}_T$  signal discussed here. As we can see, for such large integrated luminosities the  $WZ + \cancel{E}_T$  trilepton channel is competitive with general purpose searches if squarks are essentially decoupled ( $m_{\tilde{q}} \gtrsim 2 \text{ TeV}$ ) and the neutralino masses lie in the  $M_Z < m_{\tilde{Z}_2} - m_{\tilde{Z}_1} < m_h$  band.

### 3 The $\ell^+\ell^-jj+\cancel{E}_T$ channel

As seen in the last section, the main challenge of the trilepton signal is its small rate, which requires relatively high luminosities for observability. A way to increase the rates from  $WZ+\cancel{E}_T$  events is to consider the dilepton channel, where  $W \rightarrow jj$ . However, while the main SM background for the  $\ell^+\ell^-\ell'+\cancel{E}_T$  channel was weakly produced ( $WZ$ ), the  $\ell^+\ell^-jj+\cancel{E}_T$  channel has an irreducible  $t\bar{t}$  background, which can easily overcome the  $WZ+\cancel{E}_T$  signal due to its large cross section. Nonetheless, we will show that once evidence of a  $\widetilde{W}_1\widetilde{Z}_2$  signal has been seen in the trilepton channel, a corroborative signal (with lower significance) is expected in the dilepton channel.

Using the same signal and BG event samples discussed in Sec. 2, we extract events with a  $\ell^+\ell^-jj+\cancel{E}_T$  topology requiring:

#### Pre-Selection Cuts:

- $p_T(\ell) > 20$  GeV and  $|\eta(\ell)| < 2.5$  on isolated leptons,
- $n(jets) \geq 2$ ,
- $n(b-jets) = 0$ ,
- $n(\text{isol. leptons}) = 2$  (of OS/SF).

In Table 2, we show the cross sections after the pre-selection cuts above for the leading BG processes and the  $\widetilde{W}_1\widetilde{Z}_2$  signal for the same chargino and neutralino masses used in Table 1. As seen in the Table, after the pre-selection cuts, the SM BG is dominated by  $Z+jets$ , followed by  $t\bar{t}$ . To remove much of the background from  $Z+jets$  production, we further require:

- $\cancel{E}_T > 40$  GeV,
- $\cancel{E}_T/M_{eff} > 0.1$ ,
- $\Delta\phi(\vec{p}_{jet}, \vec{\cancel{E}}_T) > 0.4$  for the three hardest  $p_T$  jets.

After these cuts have been applied, the SM background becomes dominated by  $t\bar{t}$ , which still surpass the signal by almost two orders of magnitude, as shown in Table 2. However, we have not yet made use of the fact that, for the signal, the dijet invariant mass distribution should reconstruct to  $m(jj) \sim M_W$ . Therefore, in addition to the previous cuts, we include:

- $|m(jj) - M_W| < 20$  GeV,

where  $m(jj)$  is the invariant mass of the two highest  $p_T$  jets.

In Fig. 7, we show the  $m(\ell^+\ell^-)$  distribution for signal and background after all the above cuts have been applied. The dominant backgrounds displayed are  $t\bar{t}$  and  $Z+jets$  (including  $Z \rightarrow \tau\bar{\tau}$ ). Due to the  $\cancel{E}_T$  cut, the remaining  $Z+jets$  contribution comes mostly from  $Z \rightarrow \tau\bar{\tau}$ , with  $\tau$ s decaying leptonically. Therefore all  $Z+jets$  events have  $m(\ell^+\ell^-) < M_Z$ . For these dominant backgrounds— $t\bar{t}$ ,  $Z \rightarrow \tau\bar{\tau}$  etc.—we expect nearly equal contributions of opposite-flavor dileptons (OF):  $e^\pm\mu^\mp$  pairs, while signal is all in the SF dilepton channel. Hence the OF

	$Z + jets$	$t\bar{t}$	Total BG	Signal
Events Generated	6.9M	5.1M		200K
Total $\sigma$	$7.6 \times 10^6$	$5 \times 10^3$	$7.8 \times 10^6$	$1.1 \times 10^3$
Pre-selection	11,542	465	12,155	9.0
$\cancel{E}_T > 40$ GeV	71.1	357	453	6.4
$\cancel{E}_T/M_{eff} > 0.1$	45.8	345	415	6.2
$\Delta\phi(j, \cancel{E}_T) > 0.4$	31.0	296	346	5.3
$m(jj)$ cut	5.4	40.4	48.6	1.7
$m(\ell^+\ell^-)$ cut	0	5.9	6.5	1.6

Table 2: Number of events generated, total cross section and cross section after cuts for the dominant backgrounds and for the signal in the dilepton OS/SF channel. All cross sections are in fb and the signal corresponds to  $\tilde{W}_1\tilde{Z}_2$  production with  $m_{\tilde{W}_1} = 189.3$  GeV,  $m_{\tilde{Z}_2} = 187.3$  GeV and  $m_{\tilde{Z}_1} = 89.4$  GeV. The total BG values include all processes listed in the text, including the subdominant ones not shown in the Table.

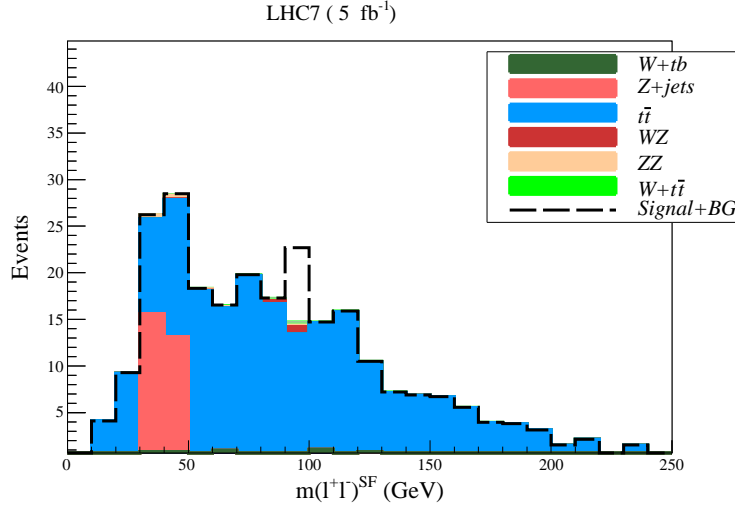


Figure 7: Number of OS/SF dilepton events expected in  $5 \text{ fb}^{-1}$  of LHC7 data versus  $m(\ell^+\ell^-)$  for various summed SM backgrounds (shaded) and signal plus BG (dashed) with  $m_{\tilde{W}_1} = 189.3$  GeV,  $m_{\tilde{Z}_2} = 187.3$  GeV and  $m_{\tilde{Z}_1} = 89.4$  GeV.

distribution can serve as a background normalization. As seen in Fig. 7, the signal is visible over the  $t\bar{t}$  distribution at  $m(\ell^+\ell^-) = M_Z$ .<sup>7</sup> Therefore, after applying the cuts listed above, we also require:

- $|m(\ell^+\ell^-) - M_Z| < 10$  GeV .

As shown in Table 2, after the  $m(\ell^+\ell^-)$  cut has been included, the BG is almost entirely given by  $t\bar{t}$ , which contribution can be estimated using the opposite-flavor dilepton invariant

<sup>7</sup>Isajet does not include the  $Z$  width smearing in the real  $Z$  emission, so all  $Z \rightarrow \ell^+\ell^-$  fall exactly at  $M_Z$ .

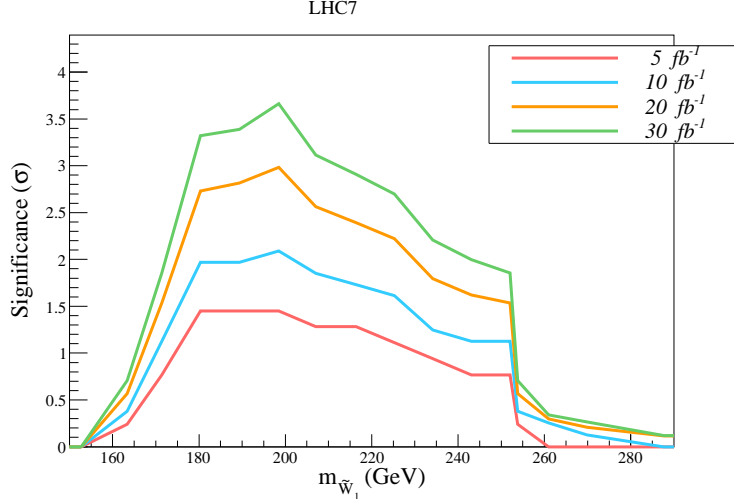


Figure 8: *Significance of  $\tilde{W}_1\tilde{Z}_2 \rightarrow WZ + \cancel{E}_T \rightarrow jj + (Z \rightarrow \ell^+\ell^-) + \cancel{E}_T$  signal for various integrated luminosities at LHC7, after the cuts listed in Table 2 have been applied.*

mass, as mentioned above. However, although the dilepton signal rate is considerably superior to the trilepton case, the signal still is significantly below the background. In Fig. 8 we plot the signal significance after the above cuts have been applied for various integrated luminosity values versus  $m_{\tilde{W}_1}$ . As in Fig. 4 we assume a mSUGRA line with  $m_0 = 10$  TeV,  $A_0 = -2m_0$ ,  $\tan\beta = 25$  and  $\mu > 0$ . We see immediately that the significance in the dilepton channel is almost half of the significance in the trilepton channel, shown in Fig. 4. Nevertheless, corroborative evidence at the  $2\sigma$  level is expected over almost the entire kinematically allowed range for an integrated luminosity of 20-30  $\text{fb}^{-1}$ .

## 4 Summary and conclusions

In this paper, we have pointed out that for a class of SUSY models with decoupled matter scalars,  $m_{\tilde{W}_1} \sim m_{\tilde{Z}_2} \lesssim m_{\tilde{g}}/3$  and gluino masses above  $\sim 500$  GeV, electroweak production of  $\tilde{W}_1\tilde{Z}_2$  dominates the SUSY production rate at LHC7. We have examined the case where  $M_Z < m_{\tilde{Z}_2} - m_{\tilde{Z}_1} < m_h$ , for which we expect the two-body decay modes  $\tilde{Z}_2 \rightarrow \tilde{Z}_1 Z$  and  $\tilde{W}_1 \rightarrow \tilde{Z}_1 W$  to dominate, leading to rather simple final state topologies including  $(Z \rightarrow \ell^+\ell^-) + (W \rightarrow \ell'\nu_{\ell'}) + \cancel{E}_T$  (trileptons) and  $(Z \rightarrow \ell^+\ell^-) + (W \rightarrow q\bar{q}') + \cancel{E}_T$  (dilepton plus jets).

Evaluation of the trilepton signal against SM backgrounds shows that the SUSY signal should be observable with a  $5\sigma$  significance at LHC7 up to  $m_{\tilde{W}_1} \sim 250$  GeV (depending on  $m_{\tilde{Z}_1}$ ), for an integrated luminosity of 30  $\text{fb}^{-1}$ . In models with gaugino mass unification, this corresponds to a range in gluino masses of  $m_{\tilde{g}} \sim 700 - 900$  GeV. Moreover, we find that for most of this region a  $\sim 2\sigma$  excess is expected in the 5  $\text{fb}^{-1}$  data sample that has already been accumulated. Assuming 30  $\text{fb}^{-1}$  of integrated luminosity at LHC7, the trilepton channel will be competitive in reach with the canonical multijet plus  $\cancel{E}_T$  search in models with unified gaugino mass parameters. If a signal is seen in the trilepton channel, a  $2 - 3.5\sigma$  confirmatory signal is



also expected in the dilepton plus jets channel for most of the parameter space, thus making a stronger case for the  $\tilde{W}_1\tilde{Z}_2$  signal. Most importantly, the simultaneous presence of these signals will point to the SUSY origin of any new physics that might be discovered in the 2012 run.

## Acknowledgments

This work was supported in part by the U.S. Department of Energy under grant Nos. DE-FG02-04ER41305, DE-FG02-04ER41291 and DE-FG02-95ER40896, by the IN2P3 of France under contract PICS FR-USA No. 5872 and by the Fundação de Apoio à Pesquisa do Estado de São Paulo (FAPESP).

## References

- [1] For a review of SUSY, see H. Baer and X. Tata, *Weak Scale Supersymmetry: From Superfields to Scattering Events*, (Cambridge University Press, 2006).
- [2] ATLAS collaboration, G. Aad *et al.*, arXiv:1109.6572, arXiv:1109.6606, JHEP 11 (2011) 99, and arXiv:1110.6189; see also <https://twiki.cern.ch/twiki/bin/view/AtlasPublic/SupersymmetryPublicResults>
- [3] CMS collaboration, S. Chatrchyan *et al.*, *Phys. Rev. Lett.* **107** (2011) 221804, CMS-PAS-SUS-11-008; see also <https://twiki.cern.ch/twiki/bin/view/CMSPublic/PhysicsResultsSUS>
- [4] A. Chamseddine, R. Arnowitt and P. Nath, *Phys. Rev. Lett.* **49**, 970 (1982); R. Barbieri, S. Ferrara and C. Savoy, *Phys. Lett. B* **119**, 343 (1982); N. Ohta, *Prog. Theor. Phys.* **70**, 542 (1983); L. J. Hall, J. Lykken and S. Weinberg, *Phys. Rev.* **D27**, 2359 (1983); For a review, see *e.g.* R. Arnowitt and P. Nath, arXiv:0912.2273 (2009).
- [5] ATLAS collaboration, ATLAS-CONF-2011-098.
- [6] H. Baer, C. H. Chen, F. Paige and X. Tata, *Phys. Rev.* **D 52** (1995) 2746.
- [7] H. Baer, C. H. Chen, F. Paige and X. Tata, *Phys. Rev.* **D 53** (1996) 6241.
- [8] H. Baer, V. Barger, D. Karatas and X. Tata, *Phys. Rev.* **D 36** (1987) 96; H. Baer, R. M. Barnett, M. Drees, J. F. Gunion, H. E. Haber, D. L. Karatas and X. R. Tata, *Int. J. Mod. Phys. A* **2**, 1131 (1987); H. Baer, A. Bartl, D. Karatas, W. Majerotto and X. Tata, *Int. J. Mod. Phys. A* **4** (1989) 4111; H. Baer, X. Tata and J. Woodside, *Phys. Rev.* **D 42** (1990) 1568; for earlier work on sparticle decays to just gauginos, see H. Baer, J. Ellis, G. Gelmini, D. V. Nanopoulos and X. Tata, *Phys. Lett. B* **161** (1985) 175; G. Gamberini, *Z. Physik C* **30** (1986) 605; H. Baer and E. Berger, *Phys. Rev.* **D 34** (1986) 1361.
- [9] H. Baer, X. Tata and J. Woodside, *Phys. Rev.* **D 41** (1990) 906 and *Phys. Rev.* **D 45** (1992) 142.
- [10] M. Dine, A. Kagan and S. Samuel, *Phys. Lett. B* **243** (1990) 250; N. Arkani-Hamed and H. Murayama, *Phys. Rev.* **D 56** (1997) 6733.

- [11] M. Drees, *Phys. Rev.* **D 33** (1986) 1468; S. Dimopoulos and G. Giudice, *Phys. Lett.* **B 357** (1995) 573; A. Pomarol and D. Tomassini, *Nucl. Phys.* **B 466** (1996) 588; A. Cohen, D. B. Kaplan and A. Nelson, *Phys. Lett.* **B 388** (1996) 588;
- [12] S. Sekmen, *et al.*, arXiv:1109.5119 [hep-ph].
- [13] W. Beenakker, R. Hopker, M. Spira, hep-ph/9611232 (1996).
- [14] S. Mrenna [For the CMS Collaboration], arXiv:1110.4078 [hep-ph].
- [15] H. Baer, V. Barger, A. Lessa, W. Sreethawong and X. Tata, arXiv:1201.2949.
- [16] H. Baer, C. H. Chen, F. Paige and X. Tata, *Phys. Rev.* **D 50** (1994) 4508.
- [17] H. Baer and X. Tata, *Phys. Rev.* **D 47** (1993) 2739.
- [18] F. Paige, S. Protopopescu, H. Baer and X. Tata, hep-ph/0312045.
- [19] M. Mangano, M. Moretti, F. Piccinini, R. Pittau and A. Polosa, *J. High Energy Phys.* **0307** (2003) 001.
- [20] J. Alwall, M. Herquet, F. Maltoni, O. Mattelaer and T. Stelzer, *J. High Energy Phys.* **1106** (2011) 128.
- [21] T. Sjostrand, S. Mrenna and P. Skands, *J. High Energy Phys.* **0605** (2006) 026.
- [22] MCFM, by J. Campbell and R. K. Ellis. See R. K. Ellis, Nucl. Phys. Proc. Suppl. **160** (2006) 170.
- [23] H. Baer, V. Barger and A. Mustafayev, arXiv:1112.3017.
- [24] H. Baer, V. Barger, A. Lessa and X. Tata, arXiv:1112.3044 [hep-ph].
- [25] H. Baer, V. Barger and P. Huang, *J. High Energy Phys.* **111** (2011) 031.
- [26] S. Bobrovskiy, F. Brummer, W. Buchmuller and J. Hajer, arXiv:1111.6005 [hep-ph].